Catal Lett (2013) 143:176–183
DOI 10.1007/s10562-012-0946-6

Monte Carlo Simulations and Theoretical Mean Field Analysis of Two Sites in the Oxidation of CO Over $Cu_{0.1}Ce_{0.9}O_{2-y}$ with Oxygen Supplied as the Gas and from the Catalyst's Bulk

Joaquín Cortés · Eliana Valencia · Paulo Araya

Received: 3 October 2012 / Accepted: 28 November 2012 / Published online: 14 December 2012

Abstract A kinetic Monte Carlo simulation algorithm and a theoretical mean field study of two sites is developed to interpret a redox mechanism based on that proposed by Sedmak et al. for the oxidation of CO over the nanostructured catalyst $Cu_{0.1}Ce_{0.9}O_{2-y}$. The simulations reproduce adequately the published experimental results and the theoretical study allows the observation of some microscopic behaviour shown by this system.

Keywords Heterogeneous catalysis · Catalysis, CO oxidation · Processes and reactions, Monte Carlo · Mean field theory

1 Introduction

Traditionally the catalytic oxidation of CO has used noble metals (Rh, Pt and/or Pd) and cerium oxide as promoter [1–3] This reaction has been of great interest, forming part of so-called three-way catalysts (TWCs) in automobiles and more recently in the WGS reaction due to the serious pollution problems caused by the use of fuels cells, currently of great interest. Recently, use has also been made of Cu with good results [4–7] In this case the promoting effect of CeO_2 has been related to a synergic effect of the system's redox properties which is achieved by the formation of copper–ceria interactions.

Another interesting aspect of this type of catalysts is their property of storing the oxygen in the bulk, allowing its production of that necessary for the oxidation if the environment is poor in it and storing it if its production increases. Recently, Sedmak et al. [8] have published studies on the oxidation of CO (CO/O_2 reaction) using the nanostructured catalyst $Cu_{0.1}Ce_{0.9}O_{2-y}$ when the O_2 is supplied from the gas phase, continuing the work of the group of Martínez-Arias on similar systems [9] and also with the oxygen being supplied from the bulk of the catalyst [10] or alternately supplied from the gas phase and from the bulk [11]. As shown by Polster et al. [12], if the Cu load is not too high, the X-ray diffraction peak positions of these catalysts are identical to those of pure fluorite CeO_2. Their experiments also show that most surface Cu species are in the form of Cu–O–Ce species.

With the purpose of observing and analyzing the microscopic behaviour of various situations studied in this system, we have used Monte Carlo (MC) simulation techniques and theoretical mean field calculations of the kinetic mechanism of the corresponding catalytic reaction. For the adequate theoretical interpretation of the reactions of the redox mechanism of this system it was necessary to establish a scheme of two sites similar to one published earlier by Polster et al. [12] and also by us for the CO–NO reaction [13]. In the following we will show the results of the MC simulation, followed by the mean field calculations for this reaction.

2 Kinetic Mechanism of the $CO–O_2$ Reaction Over $Cu_{0.1}Ce_{0.9}O_{2-y}$

There is agreement in the literature that the kinetic mechanism of the oxidation of CO over $Cu_{0.1}Ce_{0.9}O_{2-y}$ takes

J. Cortés (✉) · P. Araya
Departamento de Ing. Química, Facultad Ciencias Físicas y Matemáticas, Universidad de Chile,
Casilla 2777, Santiago, Chile
e-mail: jcortesgarrido@ing.uchile.cl

E. Valencia
Departamento Ciencia de los Materiales, Facultad Ciencias Físicas y Matemáticas, Universidad de Chile,
Casilla 2777, Santiago, Chile

place through a redox or Mars von Krevelen (MK) type mechanism [14]. It can be represented, through a simple two-step scheme in which the oxidized catalyst is reduced with CO, yielding the product directly, and then the reduced catalyst is oxidized with O_2, recovering the original oxidized catalyst. Through this simplified mechanism Sedmak et al. [8] interpreted the data of the system of concern to us in the case in which the required oxygen for the oxidation comes from the gas phase.

However, the full mechanism is more complex, including additional steps such as those shown in Scheme 1 below. The first six steps of the scheme were proposed by Sedmak et al. [10, 11] for the case in which the oxygen is supplied only from the catalyst's bulk. We have also included two additional steps to describe the catalyst's oxidation when the oxygen comes from the gas phase, and two more to consider the reverse processes corresponding to the bulk oxidation.

The mechanism of Sedmak et al. [10, 11] is based on one proposed somewhat earlier by Martínez-Arias et al. [9] which assume that production occurs directly through an Eley–Rideal type process between the CO of the gas phase and the oxidized catalyst, causing the reduction of the latter. On the other hand, the Scheme 1 includes, in contrast with the mechanism of Martínez Arias, the intermediate species formed by catalyst particles oxidized and reduced by the adsorbed CO. CO_2 is produced in step 2 only by the decomposition of the oxidized particles containing CO, while the reduced species containing CO can be oxidized from the bulk during steps 4 and 5, or from the gas phase during steps 6 and 7. In steps 8 and 9 we have also described the recovery of bulk oxygen from the oxygen of the gas phase.

$$1)\ CO + Cu^{2+} - O - Ce^{4+} \xrightarrow{k_1} CO\cdots Cu^{2+} - O - Ce^{4+}$$

$$2)\ CO\cdots Cu^{2+} - O - Ce^{4+} \xrightarrow{k_2} CO_2 + Cu^{+} - V_O - Ce^{3+}$$

$$3)\ CO + Cu^{+} - V_O - Ce^{3+} \xrightarrow{k_3} CO\cdots Cu^{+} - V_O - Ce^{3+}$$

$$4)\ Ce^{4+} - O_b + V_{ss} \xrightarrow{D} Ce^{3+} - V_b + O_{ss}$$

$$5)\ CO\cdots Cu^{+} - V_O - Ce^{3+} + O_{ss} \xrightarrow{k_5} CO\cdots Cu^{2+} - O - Ce^{4+} + V_{ss}$$

$$6)\ \{CO\cdots\}Cu^{+} - V_O - Ce^{3+} + O_2 \xrightarrow{k_6} \{CO\cdots\}Cu^{+} - O_2 - Ce^{3+}$$

$$7)\ \{CO\cdots\}Cu^{+} - O_2 - Ce^{3+} + \{CO\cdots\}Cu^{+} - V_O - Ce^{3+} \xrightarrow{k_7} \{CO\cdots\}Cu^{2+} - O - Ce^{4+} + \{CO\cdots\}Cu^{2+} - O - Ce^{4+}$$

$$8)\ \{CO\cdots\}Cu^{2+} - O - Ce^{4+} + V_{ss} \xrightarrow{D} \{CO\cdots\}Cu^{+} - V_O - Ce^{3+} + O_{ss}$$

$$9)\ Ce^{3+} - V_b + O_{ss} \xrightarrow{D} Ce^{4+} - O_b + V_{ss}$$

Scheme 1 Mechanism of the CO–O_2/$Cu_{0.1}Ce_{0.9}O_{2-y}$ reaction used in the Monte Carlo simulations (CO··· represents CO adsorbed on copper,{CO···} Cu represents copper that may or may not have adsorbed CO, V_0 is a vacant surface site, V_b in the bulk, V_{ss} in the subsurface, O_b is an oxygen in the bulk, and O_{ss} is an oxygen in the subsurface.)

In this work, Scheme 1 has been used to establish the Monte Carlo algorithm that simulates two situations: (a) the oxidation of the catalyst with oxygen coming only from the bulk (steps 1–5), and (b) the oxidation with oxygen coming from both the bulk and the gas phase (steps 1–9). This allows replicating and commenting the experimental results published by Sedmak et al. [10, 11] for the two cases.

In the second part of the paper we have made the mean field calculations of the system's kinetic equations using the kinetic mechanism represented in Scheme 2, to describe and discuss conceptually the microscopic behaviour of the system when the oxygen comes from the gas phase. Steps 1 and 2 of Scheme 2 represent steps 3 and 1 of Scheme 1, respectively, while step 3 of CO_2 production is identical to step 2 of Scheme 1. The final two steps, as represented by Sedmak et al. [8] show the reoxidation of the catalyst by the oxidant Ox–O (in this case O_2), which donates an oxygen atom to the catalyst and is thereby reduced. The possibility of direct desorption of CO in the reverse reactions of the two first steps has also been included, as proposed by Martínez-Arias et al. [9] in the case of the oxidized particle.

3 Monte Carlo Simulation of the CO–O_2/$Cu_{0.1}Ce_{0.9}O_{2-y}$ Reaction

Continuing with previous work in our laboratory on MC studies of various systems [13, 15–17], a MC simulation algorithm was developed for the CO/O_2 reaction over $Cu_{0.1}Ce_{0.9}O_{2-y}$ in two cases: in the first oxygen is supplied completely from the catalyst's bulk, while in the second is mainly supply by the gas phase. For this purpose use was made of the reaction mechanism shown in Scheme 1. The catalyst's surface was simulated consisting on (111) crystal face, which is experimentally the most frequent in cerium oxide CeO_2. Considering the experiments and conclusions of Polster et al. [12], both the methods of synthesis of the catalyst, e.g., co-precipitation to obtain a high degree of mixing between the CuO and CeO_2 phases, as well as its characterization, suggest that the natural way of modelling the location of the Cu atoms on the surface would be a

$$1)\ Cat + CO \xleftrightarrow{k_1,k_2} CO...Cat$$

$$2)\ Cat - O + CO \xleftrightarrow{k_3,k_4} CO...Cat - O$$

$$3)\ CO...Cat - O \xrightarrow{k_5} CO_2 + Cat$$

$$4)\ Cat + O_x - O \xrightarrow{k_6} Cat - O + O_x$$

$$5)\ CO...Cat + O_x - O \xrightarrow{k_7} CO...Cat - O + O_x$$

Scheme 2 Mechanism of the CO–O_2/$Cu_{0.1}Ce_{0.9}O_{2-y}$ reaction used for the mean field calculations (*Cat* is a surface species of the reduced catalyst, so *Cat*–O corresponds to an oxidized species. In both species CO adsorption can occur, represented by CO···*Cat* or CO···*Cat*–O.)

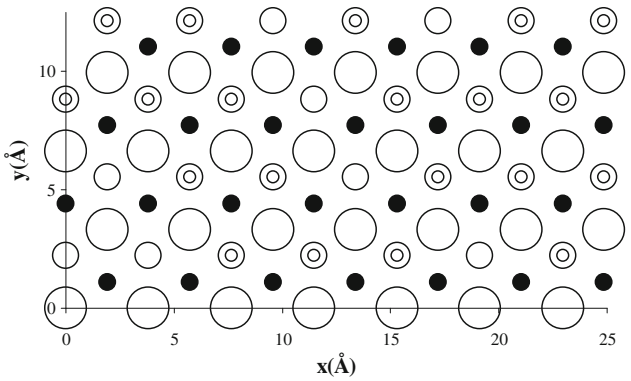

Fig. 1 Model of the catalyst's surface (face (111) of CeO_2) used in the Monte Carlo simulations. *Big open circle* oxygen, *filled circle* cerium, *small open circle* site that can contain copper, *circle within the circle* site that contains copper

random distribution of those sites, which we have placed occupying all or a fraction of the holes not occupied by cerium atoms exposed on the surface (Fig. 1).

Our simulation also takes into account the limitation established by the flow of CO or O_2 fed to the reactor. The fraction of surface considered consists of 200 × 200 atoms of each species and represents a small part (0.221×10^{-11} mg) of the catalyst's mass, so the adsorption of only a number of molecules per unit time proportional to that flow is allowed.

An important aspect of the simulation is the design of the subsurface proposed by Sedmak et al. [10] and its behaviour during the kinetic process. Such subsurface consists of a monolayer of the crystal located under the surface layer. In that layer only the sites occupied by oxygen (S'_2) are considered. In the MC algorithm the subsurface starts acting as the superficial oxygen is used, becoming the "bridge" through which the oxygen from the bulk replaces that from the surface.

Most of the constants used were obtained from Sedmak et al. [10] except the adsorption constant of O_2 and the diffusion constants D which have been assumed to be equal in steps 4, 8 and 9 of schema 1, while the dissociation constant of O_2 ($k7$), which was fitted qualitatively from the experimental information of Sedmak et al. [10] A summary of these constants is shown in Table 1.

The simulation process begins selecting an event of Scheme 1 according to the probability of the event defined by

$$p_i = \frac{k_i}{\sum k_i} \tag{1}$$

where k_i is a function of the rate constant of step i of the Scheme 1.

In the case of steps that involve a gas A (where A can be O_2 or CO), such as steps 1, 3 and 6 of Scheme 1, constant k_i is obtained from

$$k_i = k_A P_A \tag{2}$$

where P_A is the partial pressure of gas A in the gas phase. In the case of the adsorption of O_2, k_{O_2} was calculated from the collision of O_2 gas molecules with a solid surface (effusion), whose expression is

$$k_{O_2} = S_{O_2}\sigma(2\pi M_{O_2}\mathrm{RT})^{-1/2} \tag{3}$$

where $M_{O_2} = 32$ is the molar mass of O_2, S_{O_2} is the corresponding sticking coefficient ($S_{O_2} = 0.0001$ in this case), and coefficient σ is the area occupied by one mole of active sites.

We will denote S_1 the superficial sites containing Ce, S_2 the superficial sites corresponding to oxygen, which can be in its O_2 or O^{2-} forms, or which otherwise are vacant, and S_3 the sites containing copper in the oxidation states Cu^{2+} or Cu^{+}.

To consider flow limitation, and since adsorption is a very fast process, for steps 1, 3 and 6 we proceed as follows: The real time corresponding to a Monte Carlo Step (MCS), defined as the number of events equal to the number of surface sites, is determined, relating it to $\sum k_i$.

Table 1 Kinetics parameters used in the paper

	Frequency factor	Activation energy Ea (kJ mol^{-1})
Mechanism of Scheme 1		
k_1	2.1913×10^9 L mol^{-1} s^{-1}	39.6
k_2	6.3598 s^{-1}	9.7
k_3	2.2026×10^7 L mol^{-1} s^{-1}	25.8
k_5	1.5365×10^8 s^{-1}	72.9
D	7.2942×10^5 s^{-1}	70.0
k_7	3.269×10^6 s^{-1}	35.0
Mechanism of the Scheme 2		
k_1	$1{,}2005 \times 10^3$ $torr^{-1}$ s^{-1}	25.8
$k_2 = k_4$	3×10^{16} s^{-1}	117.0
k_3	$1{,}1942 \times 10^5$ $torr^{-1}$ s^{-1}	39.6
k_5	6.3598 s^{-1}	9.7
$k_6 = k_7$	$3.8666 \times 10^6/\sqrt{T(K)}$ s^{-1}	60.2

With this information and the flow of gas through the reactor, we calculate the number of gas molecules that flow through the MC sample in N, the total number of MCS involved in the MC experiment in question. N is divided into small intervals such that the number of molecules of gas A that flow in each interval is around 100. An event from mechanism 1 is then selected and the computing program analyses the situation in detail as shown in the following selected examples:

If the chosen event corresponds to the adsorption of CO over oxidized copper (step 1) and the maximum number of CO molecules allowed in the interval is not completed, a S_2 site is selected randomly. If the chosen site is occupied by O^{2-}, then the S_3 sites that are *nn* of S_2 are revised. Whether at least one Cu^{2+} is found the event continues with the revision of the S_1 sites that are *nn* of S_2, searching for Ce^{4+}. If at least one Ce^{4+} is found, the event is successful and a CO molecule is adsorbed on Cu^{2+}. If more than one Cu^{2+} or more than one Ce^{4+} is found, they are chosen randomly. CO adsorption over Cu^{+} (step 3) takes place in a manner similar to step 1.

In step 5 an oxygen from the subsurface is added to a vacant S_2 site. If this is the chosen event, an S_2 site from the surface is chosen randomly, and if it is vacant and has as *nn* at least one Ce^{3+} and one Cu^{+} containing an adsorbed CO, the process continues with the revision of the corresponding site of the subsurface located under the chosen S_2 site. If the subsurface site contains an O^{2-}, it is transferred to the surface, where the Cu^{+} is oxidized to Cu^{2+} and the Ce^{3+} is oxidized to Ce^{4+}.

Step 4 consists in the passage of oxygen from the bulk to the subsurface. From the data of Ref. [10], the number of oxygen species that can be extracted from the completely oxidized bulk is determined for our MC sample. When step 4 is selected, a S_2 site of the subsurface is chosen randomly. If this site is empty, a oxygen diffuses from the bulk with a probability proportional to the remaining fraction of oxygen from the bulk that are liable to be removed, x_O. If step 9 is the selected event, a site on the subsurface is chosen randomly, and if it contains an oxygen it will diffuse to the bulk with a probability $(1 - x_O)$.

If there is O_2 in the gas phase, the adsorption and dissociation steps of this molecule (steps 6 and 7) must also be considered. If the adsorption of O_2 is the chosen step, the procedure is analogous to that of the adsorption of CO.

4 Results and Discussion of the MC Simulations for the Mechanism of Scheme 1

Figure 2a shows the results of the production of CO_2 versus time at different temperatures, obtained from the MC simulation of the studied system when the feed has 0.01 % of CO without any O_2 in the gas phase. In general, the behaviour seen experimentally [10] is also observed qualitatively, with a maximum activity at each temperature which decreases progressively as the oxygen stored in the bulk of the catalyst also decreases, until it is finished after sufficient time.

Remarkably the peak obtained at each temperature shows splitting, with a first peak corresponding to CO_2 production from the oxygen coming from the catalyst's surface, while the second peak accounts for the CO_2 produced from the bulk oxygen that rises to the surface in steps 4 and 5, as shown in the MC experiment shown in Fig. 2b. This microscopic behaviour describes the details of the double peak commented speculatively by Sedmak et al. [10] to explain their experimental results.

Figure 3a shows the temporal evolution of CO_2 production in the same system at 200 °C and at different CO concentrations in the gas phase. Again the MC simulations show the behaviour observed in the experiments, where not only the maximum of the production peak decreases with CO concentration, but also that the maximum decreases when the time interval of the process increases, as shown by increased peak width. Figure 3b shows the effect of

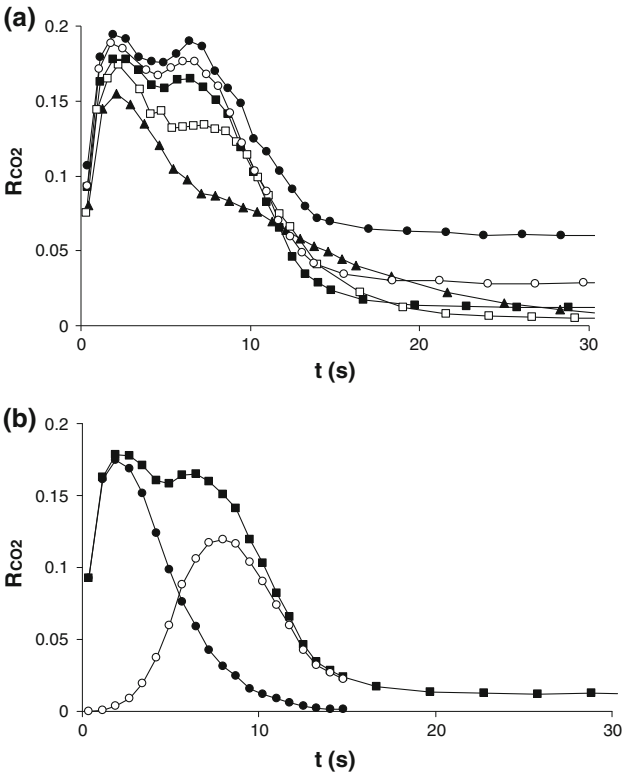

Fig. 2 Temporal evolution of production, R_{CO_2}(TON). **a** At different temperatures. CO concentration in the gas phase = 0.01 % CO. *filled triangle* 150 °C, *open square* 175 °C, *filled square* 200 °C, (*open circle*) 225 °C, (*filled circle*) 250 °C. **b** At 200 °C as a function of the origin of the oxygen. *Filled square* total R_{CO_2}, *filled circle* R_{CO_2} from the surface, *open circle* R_{CO_2} from the bulk

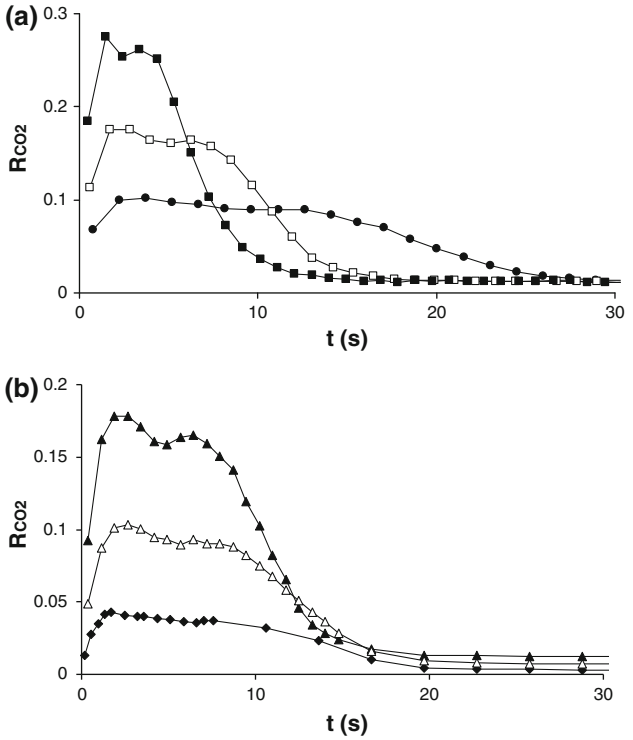

Fig. 3 Temporal evolution of production, R_{CO_2}(TON), at 200 °C. **a** At different CO concentrations *filled circle* 0.005 %, *open square* 0.01 %, *filled square* 0.02 %. **b** At different fractions of superficial copper *filled triangle* 100 %, *open triangle* 50 %, *filled diamond* 20 %

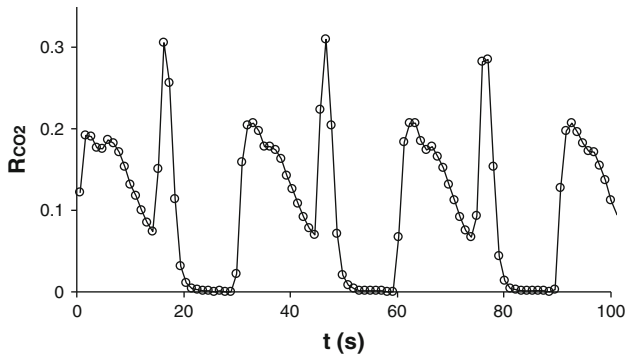

Fig. 4 Production, R_{CO_2}(TON), for cyclic changes of the reactants in the gas phase during the temporal evolution of the reaction at 258 °C; 30 s cycles (15 s 0.01 % CO and 15 s 0.01 % O_2)

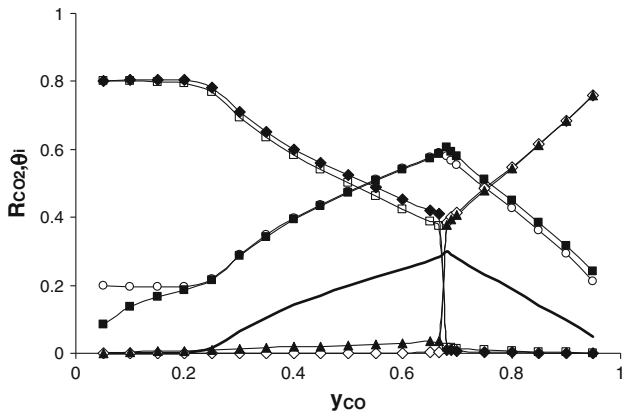

Fig. 5 Phase and production diagrams determined from Monte Carlo simulations $T = 200$ °C, total pressure = 30 (torr), *dashed line* R_{CO_2}(TON), *open circle* O, *filled diamond* O_2, *open diamond* vacant sites, *open square* Cu^+, *filled triangle* $Cu^+\cdots CO$, *filled square* $Cu^{2+}\cdots CO$

changing the copper load in the catalyst, represented by the percentage of copper seen on the surface, showing higher activity of the oxidation process as the copper load increases.

The simulation shown in Fig. 4 replicates fairly well the experimental results obtained by Sedmak et al. [11] which consist of a chain of cyclic changes corresponding to the square wave variation of the concentrations of both reactants, CO and O_2, in the gas phase. This is done, both in the experiment and in the simulation, by cutting off alternately one of the components in the gas and determining the production of CO_2 versus the reaction time. This situation reproduces satisfactorily the experimental case in which the oxygen in the gas phase decreases or disappears, while the oxygen stored in the solid phase is used.

Figure 5 shows the phase diagram and the activity for the oxidation of CO over $Cu_{0.1}Ce_{0.9}O_{2-y}$. This phase diagram can be discussed according to zones defined by CO concentration intervals in the gas phase, y_{CO} [$y_{CO} = P_{CO}/(P_{CO} + P_{O_2})$]. Zone I corresponds to $y_{CO} < 0.2$ with low CO concentrations, where no production is seen because the surface is poisoned with atomic and molecular oxygen in a distribution that does not allow the reaction, and there is a certain amount of adsorbed CO corresponding to the superficial species $CO\cdots Cu^{2+}$–O–Ce^{4+}. Atomic oxygen and $CO\cdots Cu^{2+}$ start increasing at the beginning of zone II ($0.2 < y_{CO} < 0.66$). The increase is continuous in the entire zone until a maximum at $y_{CO} = 0.66$, corresponding to the stoichiometric relation of the (CO/O_2) ratio for the $2CO + O_2 = 2CO_2$ reaction. The same behaviour is observed in the production curve, which also shows a maximum for the same value of y_{CO}. Zone II also shows a decrease of the superficial O_2 fraction. This is due to the dissociation of oxygen, which accounts for the corresponding increase of the atomic oxygen fraction and the subsequent increase of CO_2 production. The Cu^+ fraction, not included in Fig. 5, is almost identical to the O_2 fraction. Zone III, defined for $y_{CO} > 0.66$, shows a continuous decrease of production and of the atomic oxygen fraction because there is a stoichiometric excess of CO that remains on the surface in the form of $CO\ldots Cu^+$–V_0–Ce^{3+}.

5 Mean Field Model of the CO–O_2/$Cu_{0.1}Ce_{0.9}O_{2-y}$ Reaction of the Kinetic Mechanism of Scheme 2 with Oxygen Supplied from the Gas Phase

In general, the mean field kinetic models allow the generation of solutions away from the steady state. This is, usually done solving the system of differential equations corresponding to the rates of the reaction species as a function of time, (e.g., Cortés et al. [18, 19]) or in papers by Ertl et al. [20, 21] where the formation of spatio-temporal concentration patterns are interpreted. It is also possible to generate steady state solutions as described below, which correspond to solutions of the differential equations for sufficiently long times.

6 Analytical Solution of the Steady State

The mechanism of Scheme 2 corresponds to the overall oxidation reaction: $2CO + O_2 \rightarrow 2CO_2$. In a redox mechanism like the one presented here, the sites that oxygen will occupy when the surface is oxidized are different from those that CO will occupy when it is adsorbed. This makes difficult stating the kinetic equations in the way in which it is usually done with an LH mechanism in which there is only one kind of vacant sites. This would also imply that the CO and O species would compete for the same kinds of sites. In a redox mechanism this is not the case. To express that the metal is the natural site for the adsorption of CO, while the oxygen must have a different site available since it is recovered by the lattice, can be write the following normalization equations:

$$\theta_{S_1} + \theta_O = 1 \tag{4}$$

$$\theta_{S_2} + \theta_{CO} = 1 \tag{5}$$

where S_1 are the empty sites that can be oxidized with one oxygen atom and S_2 are those where a CO molecule can be adsorbed; θ_i represents the fraction of the surface covered with species i (superficial O and CO particles and empty sites S_1 and S_2). A similar solution was proposed by Cortés et al. [13] to explain the lack competition between CH_4 and O_2 in the oxidation of methane, and by Polster et al. [12] for the PROX reaction.

The rates of the overall reaction species according to the mechanism can be described by the following equations:

$$V_{CO} = -k_1 P_{CO}\theta_{S_1}\theta_{S_2} - k_3 P_{CO}\theta_{S_2}\theta_O + k_2\theta_{CO}\theta_{S_1} + k_4\theta_{CO}\theta_O \tag{6}$$

$$V_{O_2} = -k_6 P_{O_2}\theta_{S_2}\theta_{S_1} - k_7 P_{O_2}\theta_{CO}\theta_{S_1} \tag{7}$$

$$V_{CO_2} = k_5\theta_{CO}\theta_O \tag{8}$$

where k_i represent the kinetic constants of the different steps of the mechanism shown in Scheme 2.

The independent equations required to obtain analytical expressions for the two variables θ_{CO} and θ_O can be obtained in the steady state from the relations between the rates V_i corresponding to the stoichiometry of the overall reaction ($V_{CO_2} = -2V_{O_2}$ and $V_{CO_2} = -V_{CO}$) and the normalization relations (4) and (5), which must comply with the superficial fractions θ_i. This allows writing the following system of equations:

$$k_5\theta_{CO}\theta_O = 2k_6 P_{O_2}(1-\theta_O)(1-\theta_{CO}) + 2k_7 P_{O_2}\theta_{CO}(1-\theta_O) \tag{9}$$

$$k_5\theta_{CO}\theta_O = k_1 P_{CO}(1-\theta_O)(1-\theta_{CO}) + k_3 P_{CO}(1-\theta_{CO})\theta_O + k_2\theta_{CO}(1-\theta_O) + k_4\theta_{CO}\theta_O \tag{10}$$

The solution of such system of equations gives the surface fractions θ_i required to get the rates V_i of the process as a function of the kinetic constants k_i and the pressures of the gas phase. Defining the following constants:

$$A_1 = 2k_6 P_{O_2} - 2k_7 P_{O_2} - k_5 \qquad A_2 = k_1 P_{CO} - k_3 P_{CO} + k_2 - k_4 - k_5$$
$$B_1 = 2k_7 P_{O_2} - 2k_6 P_{O_2} \qquad B_2 = k_1 P_{CO} + k_2$$
$$C_1 = 2k_6 P_{O_2} \qquad C_2 = k_1 P_{CO} - k_3 P_{CO}$$
$$D_1 = 2k_6 P_{O_2} \qquad D_2 = k_1 P_{CO}$$

Equations (9) and (10) can be re-written as:

$$A_1\theta_{CO}\theta_O + B_1\theta_{CO} - C_1\theta_O + D_1 = 0 \tag{11}$$

$$A_2\theta_{CO}\theta_O + B_2\theta_{CO} - C_2\theta_O + D_2 = 0 \tag{12}$$

leading to Eq. (13), which is the expression of θ_O from Eqs. (11) and (12):

$$\theta_O = (B_1\theta_{CO} + D_1)/(C_1 - A_1\theta_{CO}) = (B_2\theta_{CO} - D_2)/(A_2\theta_{CO} - C_2) \tag{13}$$

This is a second degree equation for θ_{CO} of the form

$$A\theta_{CO}^2 + B\theta_{CO} + C = 0 \tag{14}$$

where

$A = A_2B_1 + A_1B_2$, $B = A_2D_1 - B_1C_2 - B_2C_1 - A_1D_2$, and $C = C_1D_2 - C_2D_1$

The second solution of Eq. (14) gives a physically valid value for θ_{CO}:

$$\theta_{CO} = \left(-B - \left(B^2 - 4AC\right)^{0.5}\right)\Big/2A \tag{15}$$

θ_O is then obtained from Eq. (13), while Eq. (8) is used for the activity of the process.

7 Some Numerical Results for the Mechanism of Scheme 2

Figures 6 and 7 show some numerical results for the mechanism solved in the previous section using the kinetic constants chosen for this work (Table 1). Values published by Sedmak et al. [10] have been used for the first three direct reactions of the mechanism. For the activation energy of the last two reactions, for which we have assumed the same rate constant, we have used a value given by Sedmak et al. [8] from another reference using a frequency factor, included in Table 1, calculated from the kinetic theory of gases. For the parameters of the constants of the first two reverse reactions, which we have assumed to be the same, we have used the typical values of desorption constants from metallic particles [22–24].

Figure 6a shows the results of the phase (fractions of superficial species) and production R_{CO_2}(TON) diagram versus the CO fraction in the gas phase of the system. The figure strongly suggest that production has a maximum which at higher temperatures shifts to higher values of y_{CO} (y_{COmax}). At 200 °C the production curve shows a linear shape qualitatively similar to that seen in the MC simulations (Fig. 5). The last two results are not shown in the diagram. A maximum for the activity is expected considering that the activity must decrease at high CO concentrations in the gas ($y_{CO} > y_{COmax}$) because even though on the surface there is a large amount of CO, the oxygen required for the oxidation reaction decreases until it disappears. The activity decrease at the other end of the diagram, ($y_{CO} < y_{COmax}$), occurs due to the opposite effect. Figure 6b and c show the oxidation rates versus the pressure of one of the reactants, keeping the other constant. These results illustrate the different shapes of the curves for the cases in which the pressure of CO or O_2 remains constant. These results can be explained observing the values of the superficial fractions, which are included in the graphs together with the values of y_{CO}, if activity as a function of the covered fractions, is considered (Eq. 8).

Figure 7 shows the values of the activity and the fraction of covered surface of the various superficial species as a

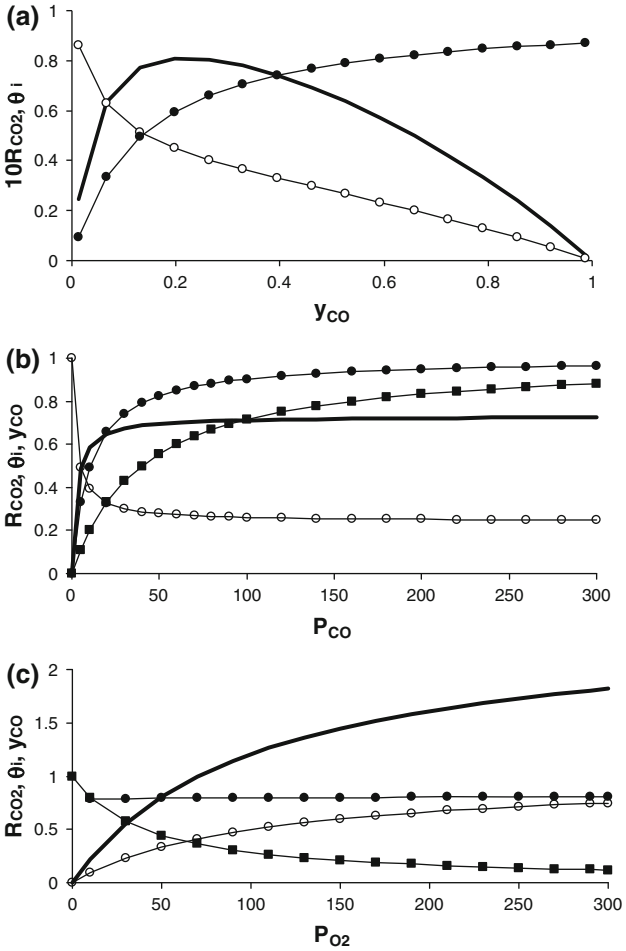

Fig. 6 **a** Phase and production diagrams determined from mean field calculations $T = 110$ °C, Total pressure = 76 (torr). **b** Variation of R_{CO_2}(TON), the fractions of covered surface θ_i and y_{CO} as a function of P_{O_2} with a fixed $P_{CO} = 40$ torr, $T = 110$ °C. **c** The same as **b** as a function of P_{CO} with a fixed $P_{O_2} = 40$ torr. *Dashed line* R_{CO_2}, *filled square* y_{CO}, *open circle* O, *filled circle* CO

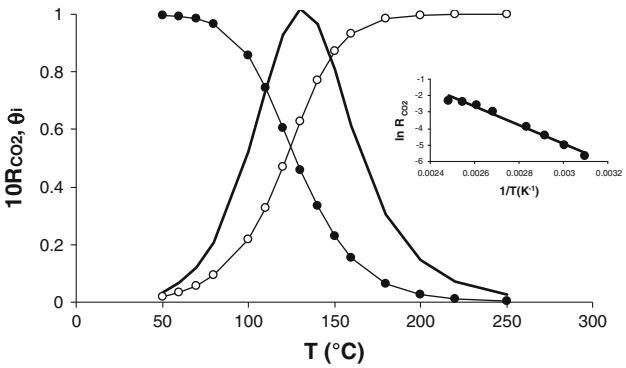

Fig. 7 Variation of R_{CO_2} and of the fraction of covered surface with temperature. Total pressure = 76 torr, $y_{CO} = 0.4$, *dashed line* R_{CO_2}, *filled circle* θ_{CO}, *open circle* θ_O. The *inset* shows Arrhenius plot $T < T_{max}$ (correlation = 0.996)

function of reaction temperature (with fixed $y_{CO} = 0.4$). A maximum of the activity of the kinetic process is seen at a temperature of 130 °C, while at both extremes the activity decreases. At $T < T_{max}$, CO coverage reaches the maximum ($\theta_{CO} = 1$), but oxygen coverage strongly decreases. At $T > T_{max}$, it is oxygen coverage that tends to a maximum ($\theta_O = 1$), while CO coverage decreases until it vanishes. This shows that the catalyst tends to be oxidized at high temperatures and reduced at low temperatures, as has been found experimentally. The inset in Fig. 7 shows that the model display good Arrhenius behaviour under the conditions used, with a correlation of 0.985 in the zone in which the activity increases with temperature ($T < T_{max}$), with an apparent energy of 11.3 kcal mol^{-1}, a value that is reasonable for this process within the interval of experimental values shown by Liu et al. [25] (8–13 kcal mol^{-1}) for the oxidation of CO over different catalysts similar to the one that we are studying.

8 Conclusions

A Monte Carlo algorithm has been developed for the oxidation of CO over $Cu_{0.1}Ce_{0.9}O_{2-y}$ that qualitatively interprets well the experimental results reported by Sedmak et al. [10, 11] such as (a) the temporal evolution of the activity at different CO concentrations, (b) at the different Cu loads, and (c) the cyclic changes that occur when the reactant feed in the gas phase is cut off alternately at a given temperature. The simulations also allow analysing the behaviour of the system microscopically, e.g., visualizing the experimental hypothesis that the first peak of the temporal evolution corresponds to superficial oxygen and the second to bulk oxygen.

The steady state behaviour of the system has been studied theoretically through a mean field scheme of two superficial sites showing, among other aspects, activity maxima versus CO concentration and temperature, and a good Arrhenius behaviour with an apparent activation energy of 11.3 kcal mol^{-1}, on the order of the (8–13) kcal mol^{-1} found experimentally.

Acknowledgments Financial support of this work through FONDECYT Project 1.110.184 is gratefully acknowledged.

References

1. Trovarelli A (1996) Catal Rev Sci Eng 38:439 and references therein
2. Fornasiero P, Di Monte R, Ranga Rao G, Kaspar J, Meriani S, Trovarelli A, Graziani M (1996) J Catal 164:173
3. Overbury SH, Huntley DR, Mullins DR, Glavee GN (1996) Catal Lett 51:133
4. Kundakovic L, Flytzani-Stephanopoulos M (1998) J Catal 179:203
5. Liu W, Sarofim AF, Flytzani-Stephanopoulos M (1994) Chem Eng Sci 49:4871
6. Luo MF, Zhong YJ, Yuan XX, Zheng XM (1997) Appl Catal A 162:121
7. Martínez-Arias A, Soria J, Cataluña R, Conesa JC, Cortés CV (1998) Stud Surf Sci Catal 116:591
8. Sedmak G, Hočevar S, Levec J (2003) J Catal 213:135
9. Martínez-Arias A, Fernández-Garcia M, Gálvez O, Coronado JM, Anderson JA, Conesa JC, Soria J, Munuera G (2000) J Catal 195:207
10. Sedmak G, Hočevar S, Levec J (2004) J Catal 222:87
11. Sedmak G, Hočevar S, Levec J (2004) Top Catal 30–31:1–4
12. Polster CS, Nair H, Baertsch CD (2009) J Catal 266:308
13. Cortés J, Valencia E, Araya P (2010) J Phys Chem C 114:11441
14. Mars P, van Krevelen DW (1954) Chem Eng Sci (Special Supplement) 3:41
15. Cortés J, Puschmann H, Valencia E (1997) J Chem Phys 106:1467
16. Cortés J, Valencia E (2003) Phys Rev E 68(1):016111
17. Cortés J, Valencia E (2004) J Phys Chem B 108(9):2979
18. Cortés J, Puschmann H, Valencia E (1996) J Chem Phys 105:6026
19. Cortés J, Puschmann H, Valencia E (1998) J Chem Phys 109:6086
20. Krischer K, Eiswirth M, Ertl G (1992) J Chem Phys 96:9161
21. von Oertzen A, Mikhailov AS, Rotermund HH, Ertl G (1998) J Phys Chem B 102:4966
22. Oh SH, Fisher GB, Carpenter JE, Goodman DW (1986) J Catal 100:360
23. Imbihl R, Cox MP, Ertl G (1985) J Chem Phys 83:1578
24. Wehner S, Baumann F, Kuppers J (2003) Chem Phys Lett 370:126
25. Liu W, Flytzani-Stephanopoulos M (1995) J Catal 153:317